

The Infrared Absorption Spectrum of Phenylacetylene and its Deuterated Isotopologue in the Mid- to Far-IR

Vincent J. Esposito,^{1, a)} Piero Ferrari,² Wybren Jan Buma,^{2,3} Ryan C. Fortenberry,⁴ Christiaan Boersma,¹ Alessandra Candian,⁵ and Alexander G. G. M. Tielens^{6,7}

¹⁾*NASA Ames Research Center, MS 245-6, Moffett Field, CA 94035, USA*

²⁾*Radboud University, Institute for Molecules and Materials, HFML-FELIX, 6525 ED Nijmegen, The Netherlands*

³⁾*Van't Hoff Institute for Molecular Sciences, University of Amsterdam, 1098 XH Amsterdam, The Netherlands*

⁴⁾*Department of Chemistry & Biochemistry, University of Mississippi, University, MS 38677-1848, USA*

⁵⁾*Anton Pannekoek Institute for Astronomy, University of Amsterdam, 1098 XH Amsterdam, The Netherlands*

⁶⁾*Leiden Observatory, Leiden University, 2333 CA Leiden, The Netherlands*

⁷⁾*Astronomy Department, University of Maryland, College Park, MD 20742-2421, USA*

(Dated: 23 February 2024)

Anharmonicity strongly influences the absorption and emission spectra of polycyclic aromatic hydrocarbon (PAH) molecules. Here, IR-UV ion-dip spectroscopy experiments together with detailed anharmonic computations reveal the presence of fundamental, overtone, as well as 2- and 3-quanta combination band transitions in the far- and mid-infrared absorption spectrum of phenylacetylene and its singly deuterated isotopologue. Strong absorption features in the 400-900 cm^{-1} range originate from CH(D) in-plane and out-of-plane wags and bends, as well as bending motions including the $\text{C}\equiv\text{C}$ and CH bonds of the acetylene substituent and the aromatic ring. For phenylacetylene, every absorption feature is assigned either directly or indirectly to a single or multiple vibrational mode(s). The measured spectrum is dense, broad, and structureless in many regions but well characterized by computations. Upon deuteration, large isotopic shifts are observed. At frequencies above 1500 cm^{-1} for d_1 -phenylacetylene, a one-to-one match is seen when comparing computations and experiment with all features assigned to combination bands and overtones. The $\text{C}\equiv\text{C}$ stretch observed in phenylacetylene is not observed in d_1 -phenylacetylene due to a computed 40-fold drop in intensity. Overall, a careful treatment of anharmonicity that includes 2- and 3-quanta modes is found to be crucial to understand the rich details of the infrared spectrum of phenylacetylene. Based on these results, it can be expected that such an all-inclusive anharmonic treatment will also be key for unraveling the infrared spectra of PAHs in general.

^{a)}Vincent.J.Esposito@nasa.gov

I. INTRODUCTION

PAHs are a class of molecules composed of fused hexagonal rings of sp^2 -hybridized carbon atoms with hydrogens decorating the periphery, which are known to be ubiquitous in space based on their infrared emission features detected throughout many interstellar regions, i.e., the aromatic infrared bands (AIBs).^{1,2} Recently, experimental and computational studies of the infrared absorption spectra of various PAHs have revealed large anharmonic effects. Previous attempts to account for anharmonicity included the use of harmonic scaling factors.^{3–13} However, scaling factors do not account for important higher-order transitions such as combination bands and overtones, nor do they provide a good treatment of systems with a shallow minimum in their PESs.¹⁴

In cases where anharmonicity is strong, scaling factors are therefore not able to account for -and accurately predict- infrared absorption spectra, in particular for regions that can only be explained when anharmonic transitions such as combination bands are correctly taken into account.^{8,15–23} Nowadays, with the launch of the James Webb Space Telescope (JWST), very sensitive and high-resolution infrared spectral data of the PAH bands have and will continue to be delivered,²⁴ calling for the need of a deeper understanding of anharmonic effects on the vibrational spectra of PAHs, and how to take them into account into astronomical models. To do so requires a synergy between accurate computational modeling and sensitive laboratory spectroscopy experiments.

In the recent past dedicated gas-phase experiments have been performed for a number of PAHs, and these indeed reveal that for these compounds anharmonicity is essential to come to a proper interpretation of their infrared absorption spectra. For example, IR-UV ion-dip molecular beam experiments have been used to record infrared absorption spectra of neutral naphthalene, anthracene, tetracene and pentacene, showing the appearance of many combination bands in the 1600–2000 cm^{-1} region.^{17,18,25–28} Similarly, molecular beam experiments on the larger PAHs coronene, peropyrene, ovalene, and hexa(peri)benzocoronene, have shown the presence of many combination bands and overtones in both the 1600–2000 cm^{-1} and 2950–3150 cm^{-1} regions, whereas at lower frequencies (100 and 1000 cm^{-1}) fundamental transitions dominate.²⁹ Recently, using an infrared table-top laser system to cover the 3 μm spectral region, our research group performed ion-dip experiments on phenylacetylene and d_1 -phenylacetylene (the singly deuterated isotopologue of phenylacetylene with deuteration

taking place at the acetylene hydrogen),¹⁶ representing an ideal model system to assess the impact of anharmonic effects on PAHs, in particular focusing on the possibility that higher-order quanta modes are a significant contributor to their infrared spectra. Remarkably, a major influence of 2- and 3-quanta modes arising from aromatic and acetylenic C-H and C-D stretching bands is observed.³⁰ Notably, phenylacetylene was recently detected in the dark molecular cloud TMC-1 via its pure rotational transitions,³¹ making the detailed understanding of its infrared spectrum a pressing need.

In this work, the previous study is extended to the much larger 100–2300 cm^{-1} spectral range using an infrared free electron laser, thereby covering the far- and mid-infrared regions. Detailed anharmonic quantum chemical calculations are utilized to reveal the key role played by higher-order modes in shaping the infrared spectra.

II. METHODS

A. Experimental

Molecular beams of phenylacetylene and d_1 -phenylacetylene are formed by placing the liquid compounds in a reservoir kept at room temperature that is seeded with a stream of Ar gas injected at a backing pressure of 4 bar. Using a Series 9 pulsed valve from General Valve, the Ar-phenylacetylene mixtures are expanded into vacuum, forming a cold and directional molecular beam that is collimated by a 2 mm skimmer. The pulsed valve is operated at 10 Hz. After collimation, the molecular beam enters the ionization region of a reflectron time-of-flight mass spectrometer (R.M. Jordan D-850) equipped with a 40 mm dual microchannel plate (MCP) detector (Jordan Co. C-726) that has a mass resolution of $m/\Delta m = 2200$ at 100 amu. In previous studies on the same apparatus with similarly-sized molecular systems, molecular dynamic simulations were used to compute infrared spectra at different temperatures, finding good agreement with a vibrational temperature of 50 K.¹⁴ Similarly, previous estimations of the molecular beam temperature place its value in the range from 10 to 50 K.^{32,33} Values much higher than this range would lead to visible hot bands in REMPI scans, which is not the case in the spectra in this study.

To measure mass spectra, phenylacetylene is ionized using a (1+1) Resonance Enhanced Two-Photon Ionization (R2PI) scheme. UV excitation is performed by the second harmonic

light of a dye laser (Radiant Dye) pumped by the third harmonic of a Nd:YAG laser (InnoLas SpitLight1200) and operating on Coumarin 153 in ethanol. The laser system is tuned to the vibrationless origin of the $S_1 \leftarrow S_0$ electronic transition of each species occurring at 35875.7 and 35888.6 cm^{-1} for phenylacetylene and d_1 -phenylacetylene, respectively.³⁰

Infrared spectra are measured by ion-dip spectroscopy. For this, the laser light of the free electron laser FELIX is aligned counter-propagating with the molecular beam as described in Ref.³⁴. Upon resonant vibrational excitation, depopulation of the vibrational ground-state leads to a reduction of the ion signal. Running the molecular beam instrument at 10 Hz and operating FELIX at 5 Hz then allows the consecutive measurement of mass spectra with and without FELIX excitation and thereby the recording of IR absorption spectra. Importantly, FELIX is timed 300 μs prior to the R2PI ionization, ensuring that vibrational excitation occurs when the molecules are in their neutral state. FELIX is tuned from 100 to 2300 cm^{-1} in steps of 1 cm^{-1} .

B. Computational

Computation of the optimized geometry; harmonic normal modes; and quadratic, cubic, and quartic normal coordinate force constants (quartic force field; QFF) is performed at the B3LYP³⁵/N07D³⁶ level of theory utilizing the Gaussian 16 software package.³⁷ The computations were done using the verytight optimization criteria and a custom integration grid consisting of 200 radial shells and 974 angular points per shell (compared to 99 radial shells and 590 angular points per shell in the default UltraFine grid) The N07D basis set is based on the 6-31G(d) basis set and contains additional diffuse and polarization functions that have been shown to increase accuracy in the anharmonic computations of large aromatic systems such as PAHs.³⁸ A QFF is a truncated Taylor series expansion of the potential surface surrounding the equilibrium geometry, following the formula:

$$\begin{aligned}
V = & \frac{1}{2} \sum_{i,j}^{3N} \left(\frac{\partial^2 V}{\partial X_i \partial X_j} \right) X_i X_j \\
& + \frac{1}{6} \sum_{i,j,k}^{3N} \left(\frac{\partial^3 V}{\partial X_i \partial X_j \partial X_k} \right) X_i X_j X_k \\
& + \frac{1}{24} \sum_{i,j,k,l}^{3N} \left(\frac{\partial^4 V}{\partial X_i \partial X_j \partial X_k \partial X_l} \right) X_i X_j X_k X_l
\end{aligned} \tag{1}$$

The QFF is computed in normal mode coordinates via a linear relationship to produce a Cartesian coordinate QFF. Additionally, semi-diagonal quartic terms are employed as is the default in Gaussian16.³⁹

From here, two different methodologies are implemented via 2nd order vibrational perturbation theory (VPT2).^{40–43} Using the built-in anharmonic frequency code within Gaussian 16, VPT2 is used to compute the anharmonic frequencies including up to three-quanta transitions. This allows for the inclusion of multi-mode combination bands that are imperative for an accurate analysis of the recorded experimental absorption data.

Alternatively, to properly treat the redistribution of intensity as a result of accidental resonances between vibrational states, a locally modified version of SPECTRO⁴⁴ is utilized to compute the anharmonic vibrational frequencies of transitions involving changes up to two vibrational quanta. SPECTRO has the advantage of using resonance polyads in the anharmonic computations.^{45,46} When two vibrational states are close in frequency and produce a near-singularity in the VPT2 treatment, they are removed from the standard perturbation treatment and included in a resonance polyad matrix. The matrix allows for the treatment of resonance effects as well as normal modes that simultaneously participate in multiple resonances. Additionally, the polyad matrix allows for the distribution of intensities between coupled vibrational states. Vibrational modes with frequencies below 300 cm⁻¹ are excluded from the SPECTRO VPT2 calculation. This method has been described previously in greater detail.^{15–19,21,25}

The resultant vibrational absorption stick spectrum is convoluted with a Gaussian line shape having a full-width at half-maximum (FWHM) of 0.5% of the computational frequency as to match the bandwidth of FELIX.

III. RESULTS AND DISCUSSION

A. Phenylacetylene Absorption Spectrum

Figure 1 presents the experimental infrared absorption spectrum (black) of phenylacetylene in the 100-2300 cm^{-1} frequency range, the harmonic stick spectrum (green), the 3-quanta anharmonic stick spectrum (purple), and the artificially broadened anharmonic spectrum (blue) based on this stick spectrum. The experimental band center, FWHM, and relative intensity along with the pertinent associated computational anharmonic mode labeling, frequency, and intensity of the pertinent bands are presented in Table III A. The full list of computational frequencies and experimental transition assignments are provided in Table S1 of the Supplementary Information (SI). The experimental transitions are determined via a least-squares fit using a Gaussian line shape. Overall, approximately 40 features can be identified from the experimental data above a signal-to-noise ratio of 2. Because of the resolution of the experiment, the many overlapping bands leads to unstructured, broad shapes and shoulders. Studying the computational spectrum leads to a deeper understanding as to why many of the features appear so broad and structure-less. For example, in the experimental spectrum the fit detected two neighboring features at 753.1 and 764.8 cm^{-1} within the broad feature centered at 753.1 cm^{-1} , which exhibits a shoulder on the high-frequency side. Using the anharmonic computations, these two features can be reliably assigned to ν_{19} (out-of-plane aromatic CH wag) and ν_{12} (in-plane aromatic ring breathing mode), respectively, clearly explaining the finer details of the 753.1 cm^{-1} feature.

Across the entirety of the spectrum (Figure 1), every experimental feature is assigned to either a single or multiple vibrational modes. Interestingly, the two features at 609.4 and 1217.6 cm^{-1} stand out as having poor agreement with the computations. The data in Table III A show that the feature centered at 609.4 cm^{-1} is assigned to ν_{21} , which is the out-of-plane (OOP) acetylene CH wag that causes a large change in the dipole moment and leads to high intensity. The difference between the experiment and computed position for this mode is 22.6 cm^{-1} , larger than expected for a fundamental mode at this level of theory, especially considering that the surrounding features are well-described by the computations (e.g., the feature at 620.6 cm^{-1} is assigned to the $\nu_{13} + \nu_{36}$ combination band computed to be at 626.7 cm^{-1}). Anharmonic computations of OOP bending motions of aromatic systems

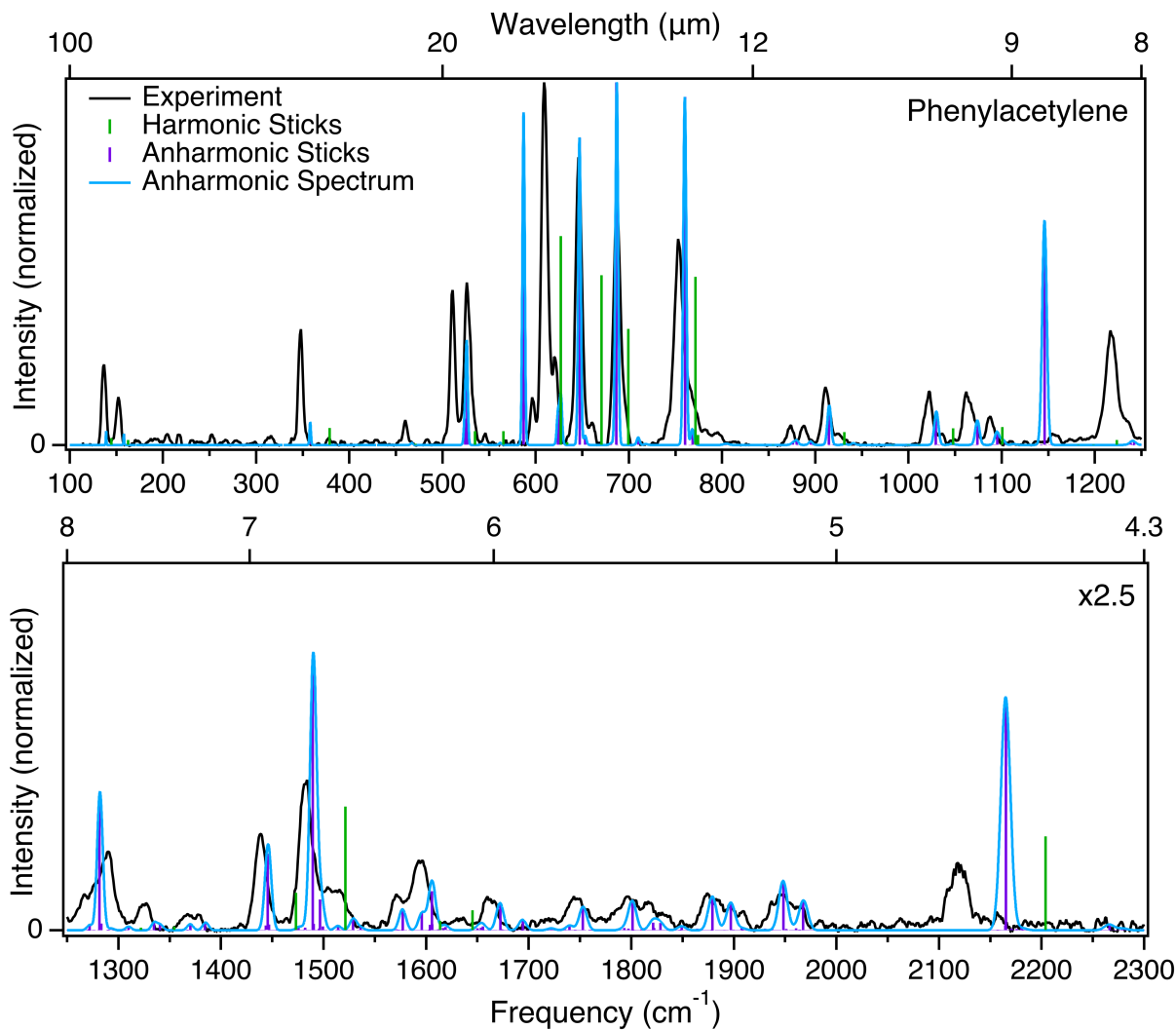


FIG. 1. Experimental (black), harmonic stick, and broadened anharmonic (blue; stick spectrum in purple) absorption spectrum of phenylacetylene. The computed anharmonic spectrum in purple represents the stick spectrum convoluted with a Gaussian function with a FWHM of 0.5% of the computational frequency to reproduce the experimental linewidth of FELIX. The intensity in the lower panel has been multiplied by a factor of 2.5 to show details of the weaker features in this region.

consisting of sp^2 hybridized carbons have been previously reported to exhibit unexpected behavior when using DFT methods in combination with some basis sets,⁴⁷. In this study, different DFT and correlated methods with varied basis sets were tested and all suffered the same issues with the OOP bending mode, and in fact, the B3LYP/N07D method performed the best against experiment. Therefore, we believe that this is indeed the cause of the

TABLE I. Phenylacetylene mode number, anharmonic computational frequency (cm^{-1}), intrinsic intensity (km mol^{-1}), and relative intensity; and the experimental band centers (cm^{-1}), FWHM (cm^{-1}), and relative intensities.

Mode	Frequency (cm^{-1})	Intrinsic Intensity (km mol^{-1})	Comp. Rel. Intensity ^a	Exp. Band Centers (cm^{-1})	FWHM Gaussian (cm^{-1})	Exp. Rel. Int.
ν_{21}	586.8	38.910	0.917	609.4	5.9	1.000
$\nu_{13}+\nu_{36}$	626.7	5.733	0.135	620.6	6.1	0.267
$\nu_{23}+\nu_{24}+\nu_{36}$	653.0	1.078	0.025	659.2	6.8	0.049
ν_{19}	760.3	40.727	0.960	753.1	8.4	0.588
ν_{12}	768.3	1.856	0.044	764.8	13.1	0.155
$\nu_{21}+\nu_{24}+\nu_{36}$	876.2	0.277	0.007	873.3	5.8	0.056
ν_{10}	1029.5	3.902	0.092	1021.8	7.8	0.138
ν_{32}	1073.9	2.855	0.067	1064.0	10.7	0.155
$\nu_{13}+\nu_{34}$	1095.3	1.536	0.036	1087.6	7.1	0.073
$2\nu_{21}$	1146.0	26.230	0.618	1217.6	11.6	0.267
ν_7	1489.6	12.538	0.296	1481.9	10.2	0.162
$2\nu_{21}+\nu_{33}$	1793.3	0.109	0.003	1795.9	18.6	0.037
$\nu_{14}+\nu_{15}$	1801.4	1.375	0.032			
$\nu_{14}+\nu_{18}$	1879.0	1.579	0.037	1875.4	15.5	0.037
$\nu_{17}+\nu_{18}$	1897.2	1.291	0.030			
$3\nu_{33}$	1907.5	0.092	0.002	1896.3	21.5	0.022
ν_5	2165.3	10.637	0.251	2119.0	18.0	0.078

^a Computational relative intensities are in reference to the transition at 686.5 cm^{-1} which is not listed here but can be found in Table S1 of the Supplementary Information

issue seen here. To confirm that there are no issues with basis set size, the harmonic vibrational spectrum of phenylacetylene calculated with B3LYP/N07D compares well to those calculated with B3LYP/6-311++G(d,p), agreeing to 16 cm^{-1} in the CH stretch region and approximately 4 cm^{-1} for lower frequency modes. The in-plane acetylene CH wag is slightly more sensitive to basis set size; however, a difference of approximately 3% will not impact the results in this study. Additionally, phenylacetylene has been reported to exhibit large couplings between various vibrational states of the acetylene substituent.³⁰ The initial error in the potential energy surface computation for ν_{21} is compounded when moving to higher-order transitions along with the general decrease in accuracy when computing the frequency of overtone transitions (see Ref.⁴⁸ for more details). This leads to a larger error in the frequency for the feature centered at 1217.6 cm^{-1} , which arises from the first overtone of ν_{21} ($2\nu_{21}$). The other feature that has poor agreement between experiment and computation

is the feature at 2119.0 cm^{-1} , assigned to ν_5 (2165.3 cm^{-1}), the acetylene $\text{C}\equiv\text{C}$ stretch. It is unclear at the moment why there is such a large difference between experiment and theory for this feature.

Moving to higher frequencies, each feature from $1250\text{-}2000\text{ cm}^{-1}$ is assigned to one or more underlying modes. Due to the congested nature of this region, some features are assigned to multiple nearby modes that cannot be separated effectively. The harmonic stick spectrum (green) in Figure 1 illustrates how important it is to include anharmonicity in the computations of the vibrational spectrum of PAHs. In the $1250\text{-}2000\text{ cm}^{-1}$ frequency range, only seven fundamental frequencies (green) exist, making it impossible to completely assign the complicated spectrum of phenylacetylene. However, when anharmonicity is included, hundreds of relatively intense overtone and combination bands present themselves that agree quite nicely with the experimental features. Furthermore, the anharmonic intensities show better agreement with the experimental intensities than the double harmonic intensities do.

Figure 2 illustrates the 2-quanta (red) and 3-quanta (blue) vibrational modes computed for phenylacetylene. The importance of including the 3-quanta modes cannot be overstated, as can be seen from the figure and is highlighted by Table III A. At least four 3-quanta modes (combination bands involving three fundamental vibrations or one fundamental mode and one overtone, as well as a second overtone mode) are assigned to features in the spectrum that would have been missed if the higher-order modes would not have been included in the computations. For example, around 1800 cm^{-1} , the experiment reveals a double feature that can only be explained by including 3-quanta modes. Of note is that the 3-quanta computations are not performed with polyad matrices and therefore do not benefit from the proper treatment of intensity sharing. The less accurate intensities can be seen in the systematically larger intensity for almost all modes in the 3-quanta computations versus those of the 2-quanta in Figure 2. A glaring example of this is the disappearance of the $2\nu_{21}$ feature in the 3-quanta computation. As the result of many strong resonance coupling interactions, the intrinsic intensity of this mode is redistributed over various nearby features. Not utilizing a polyad matrix will also affect the frequencies of the bands in the 3-quanta computations, although to a lesser degree. These issues will be addressed in subsequent studies, when the capability to compute 3-quanta modes is developed further.

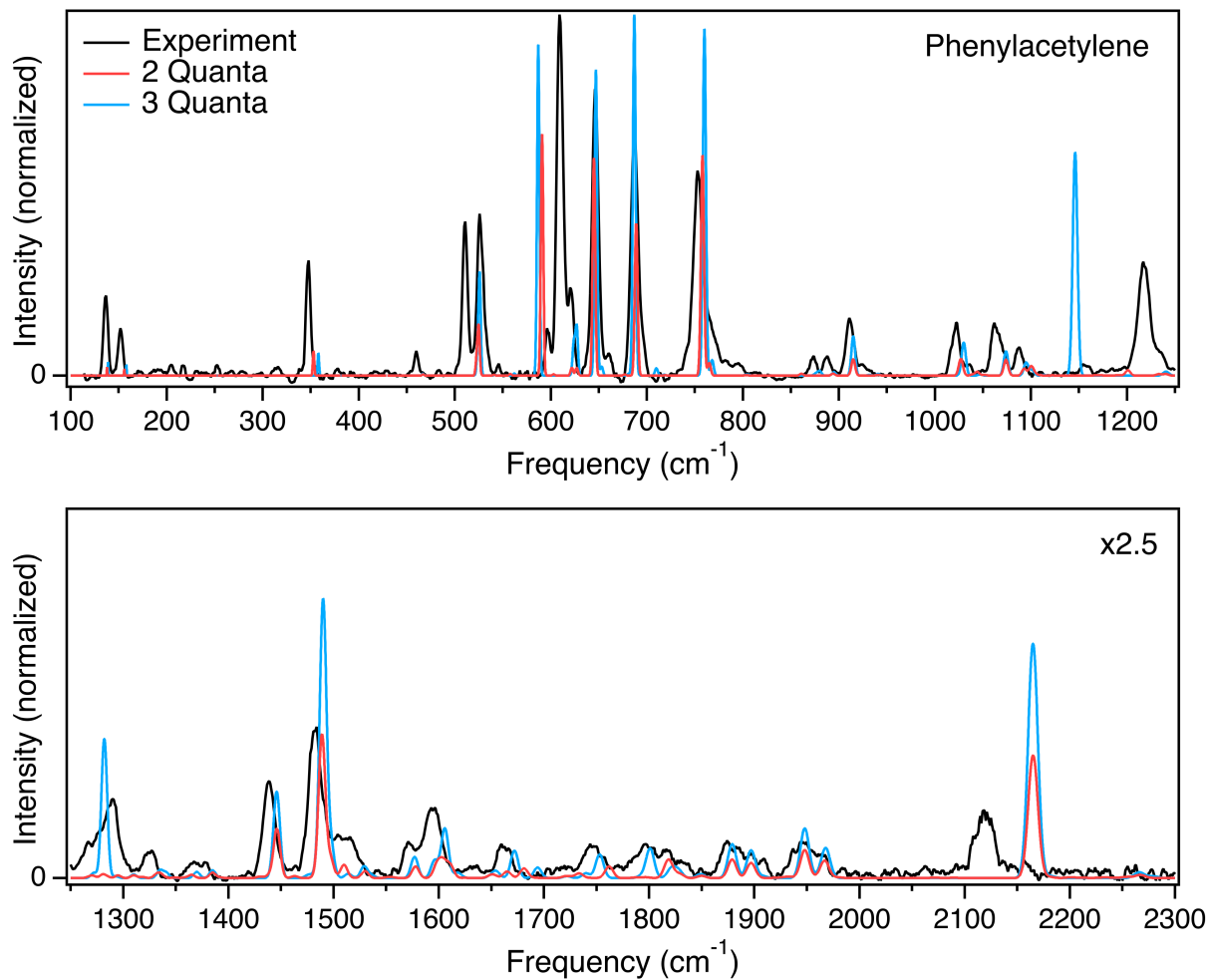


FIG. 2. Experimental (black), 3-quanta anharmonic (blue), and 2-quanta anharmonic (red) absorption spectrum of phenylacetylene. The computed 3-quanta anharmonic spectrum shown in blue is convoluted with a Gaussian line shape with a linewidth equal to 0.5% of the computational frequency, reproducing the experimental linewidth of FELIX, while the 2-quanta anharmonic spectrum shown in red has a constant 1.0 cm^{-1} FWHM (for visualization purposes). The intensity in the lower panel has been multiplied by a factor of 2.5 to show details of the weaker features in this region.

B. d_1 -Phenylacetylene Absorption Spectrum

Figure 3 presents the absorption spectrum of d_1 -phenylacetylene in the range of 100–2300 cm^{-1} with the experiment shown in black, the harmonic stick spectrum in green, the anharmonic 3-quanta stick spectrum in purple, and the anharmonic stick spectrum broad-

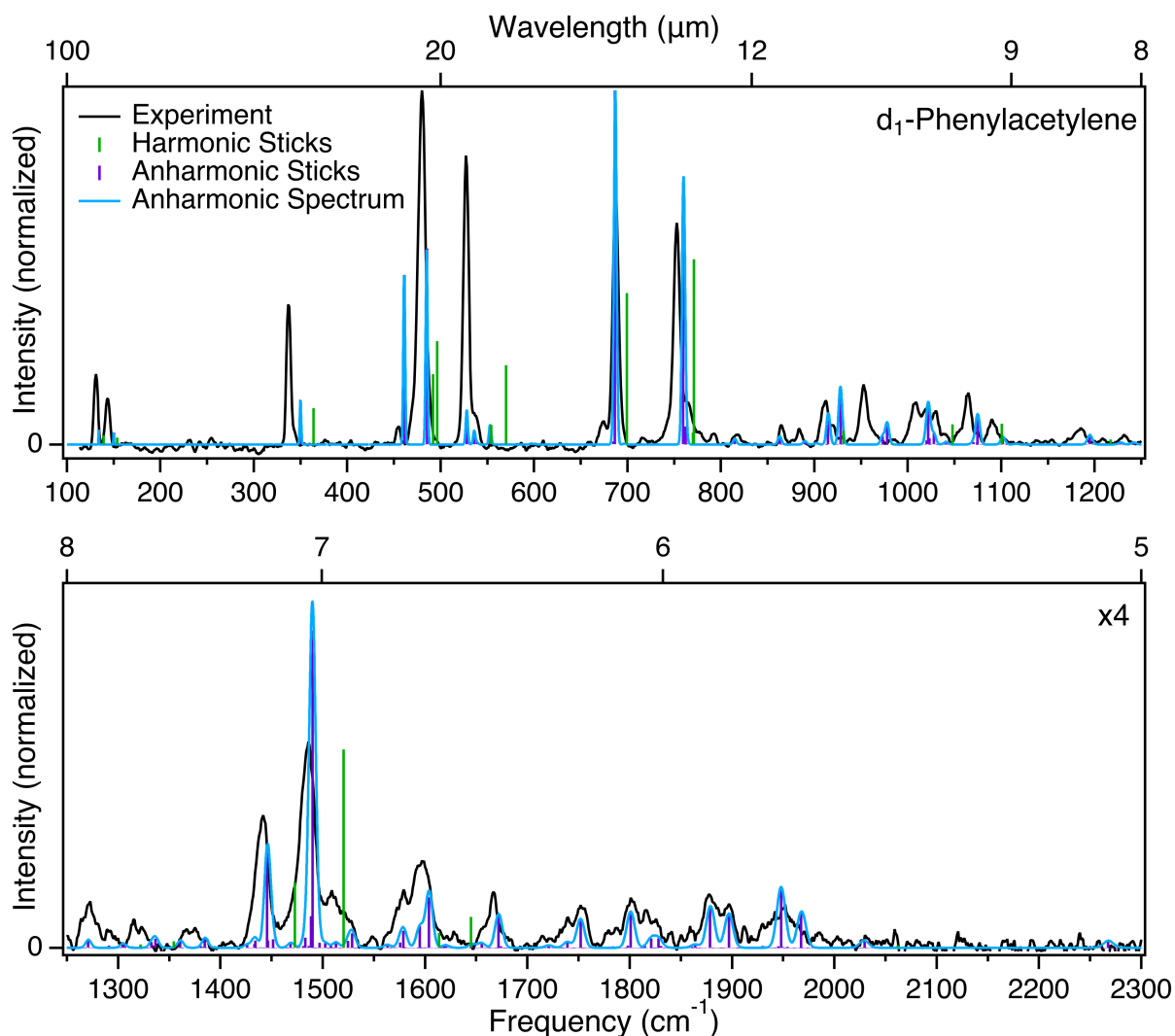


FIG. 3. Experimental (black), harmonic stick, and anharmonic (blue; stick spectrum in purple) absorption spectrum of d_1 -phenylacetylene. The computed anharmonic spectrum in blue represents the stick spectrum convolved with a Gaussian linewidth equal to 0.5% of the computational frequency to reproduce the experimental linewidth of FELIX. The intensity in the lower panel has been multiplied by a factor of 4 to show details of the weaker features in this region.

ened with a Gaussian lineshape (FWHM of 0.5% of the computational frequency) in blue. Table III B lists computational and experimental frequencies of prominent bands. The full list of experimental and computational frequencies is provided in Table S2 of the SI. In the experimental spectrum bands are observed throughout the spectral range with mostly sharp, well-defined peaks below 800 cm^{-1} and broad, structure-less features above. The sole physical difference between phenylacetylene and d_1 -phenylacetylene is a single deuteration,

but this leads to major spectroscopic changes. Many spectral shifts originate from modes that involve motion of the deuterium atom, and adjacent modes (such as the acetylene $\text{C}\equiv\text{C}$ stretch) are also impacted. Here, theory provides insights into what drives these spectral changes.

There is generally good agreement between experiment and computation across the entire spectral range with a few notable outliers. In the range from $450\text{-}560\text{ cm}^{-1}$, there are four features present in the experimental spectrum while theory predicts six bands. The three largest peaks in the experimental spectrum occur at 475.7 , 480.6 and 527.2 cm^{-1} , with the peaks at 475.7 and 480.6 cm^{-1} overlapping (Figure S1 shows an expanded view of this feature). An unambiguous assignment is difficult to make here, but the strongest peak at 480.6 cm^{-1} most likely originates from ν_{35} , which is the in-plane acetylene CD wag. ν_{22} , the OOP acetylene CD wag computed at 461.5 cm^{-1} , is tentatively assigned to the experimental feature at 475.7 cm^{-1} . This mode is analogous to ν_{21} in the standard isotopologue. Deuteration of the acetylene hydrogen leads to an experimental isotopic shift of 128.8 cm^{-1} for the OOP acetylene CH wag mode. Assigning the feature at 527.2 cm^{-1} is more difficult due to three modes computed near the central peak position and the intensity mismatch. The carrier of this peak is probably ν_{21} , the OOP acetylene $\text{C}\equiv\text{C}$ bend predicted at 528.1 cm^{-1} . After the VPT2 treatment, the computed intensity of ν_{21} drops from $18.229\text{ km mol}^{-1}$ (0.524 relative to ν_{20}) to 4.408 km mol^{-1} (0.097 relative to ν_{20}). As mentioned previously, OOP bending modes are sometimes not well described by DFT/VPT2, and intensities in general are difficult to calculate. Therefore, better agreement is found when considering the double harmonic intensities. Additionally, the lack of intensity sharing in these calculations contributes to the intensity mismatch for all of the features mentioned here. The other two small peaks predicted at 535.9 ($\nu_{16}+\nu_{24}$) and 539.1 (ν_{34}) cm^{-1} add to the intensity of the central peak, and lead as well to the appearance of the shoulder on the high frequency side.

Moving to higher frequencies, there is somewhat less agreement between experiment and computation in the $900\text{-}1100\text{ cm}^{-1}$ range. However, 10 prominent peaks are seen in both spectra, providing the ability to understand which modes are involved without directly assigning individual peaks. There is a mixture of transitions in this region characterized by fundamental, overtone, and 2- and 3-quanta combination bands contributing to features observed here; $2\nu_{22}$ reports the largest predicted intensity (see SI Table S2). Only three fundamental transitions have appreciable intensity in this region (harmonic sticks in Figure 3),

TABLE II. d₁-Phenylacetylene mode number, anharmonic computational frequency (cm⁻¹), intrinsic intensity (km mol⁻¹), and relative intensity; and experimental band centers (cm⁻¹), FWHM (cm⁻¹), and relative intensities.

Mode	Frequency (cm ⁻¹)	Intrinsic Intensity (km mol ⁻¹)	Comp. Rel. Inten- sity	Exp. Band Centers (cm ⁻¹)	FWHM Gaussian (cm ⁻¹)	Exp. Rel. Int.
ν_{22}	461.5	21.666	0.478	475.7	3.8	0.731
ν_{13}	461.7	0.245	0.005	454.3	2.0	0.079
ν_{35}	485.4	25.055	0.553	480.6	5.3	1.000
ν_{21}	528.1	4.407	0.097	527.2	4.8	0.828
$\nu_{16} + \nu_{24}$	535.9	1.785	0.039	537.2	5.8	0.082
ν_{34}	539.1	0.325	0.007			
$\nu_{21} + 2\nu_{22}$	1426.2	0.119	0.003			
$\nu_{14} + \nu_{22}$	1433.3	0.132	0.003			
$\nu_{18} + \nu_{21}$	1434.2	0.272	0.006			
ν_{28}	1445.5	3.588	0.079	1440.8	11.9	0.104
$\nu_{19} + \nu_{20}$	1446.6	0.270	0.006			
$\nu_{17} + \nu_{22}$	1451.4	0.321	0.007			
$2\nu_{21} + \nu_{22}$	1468.6	0.190	0.004			
$\nu_{13} + \nu_{34} + \nu_{35}$	1483.1	0.380	0.008			
$\nu_{10} + \nu_{13}$	1488.7	1.185	0.026	1485.1	14.7	0.160
ν_7	1490.2	11.941	0.264			
$\nu_8 + 2\nu_{36}$	1496.8	0.190	0.004	1508.8	9.5	0.043
$\nu_{13} + \nu_{20} + \nu_{23}$	1502.5	0.169	0.004			
$2\nu_{19}$	1512.9	0.209	0.005	1521.9	10.8	0.036
$2\nu_{12}$	1524.6	0.257	0.006			
$\nu_{15} + \nu_{20}$	1528.8	0.538	0.012			
$\nu_{10} + \nu_{34}$	1563.2	0.116	0.003			
$\nu_{20} + \nu_{23} + \nu_{34}$	1575.8	0.194	0.004	1576.6	12.0	0.029
ν_{27}	1578.8	0.642	0.014			
$\nu_{15} + \nu_{19}$	1594.9	0.812	0.018			
$\nu_{18} + \nu_{20}$	1603.9	0.240	0.005	1596.8	15.9	0.060
ν_6	1604.0	1.902	0.042			
$\nu_{14} + \nu_{18}$	1878.6	1.578	0.035	1879.3	13.0	0.031
$\nu_{17} + \nu_{18}$	1897.2	1.297	0.029	1896.8	8.5	0.025
ν_5	2029.5	0.277	0.006			

^a Computational relative intensities are in reference to the transition at 686.6 cm⁻¹ which is not listed here but can be found in Table S2 of the Supplementary Information

indicating and reinforcing the strong impact of anharmonicity on phenylacetylene³⁰ and the need for anharmonic computations to properly analyze and understand its spectrum.

The broad feature centered at 1440.8 cm^{-1} with a FWHM of 11.9 cm^{-1} mainly originates from the ν_{28} aromatic CH in-plane bend fundamental transition. Underlying 2- and 3-quanta combination bands account for the remaining intensity that leads to the broadness of the feature. At higher frequencies, the experimental fit identifies three overlapping peaks at 1485.1 , 1508.8 , and 1521.9 cm^{-1} that make up the double peak feature around 1500 cm^{-1} . The two main modes here are the ν_7 aromatic CH in-plane bend fundamental as well as the $\nu_{10}+\nu_{13}$ combination band transition. Other higher-order overtone and combination band transitions contribute to the broad intensity and double peak structure.

From 1550 cm^{-1} upwards, there is an almost one-to-one match of experimental and computational features, all of which are higher-order modes (see also SI Figure S2). For example, $\nu_{18}+\nu_{19}$ is the combination band responsible for the experimental peak observed at 1666.4 cm^{-1} , while $\nu_{14}+\nu_{18}$ (1878.6 cm^{-1}) and $\nu_{17}+\nu_{18}$ (1897.2 cm^{-1}) are responsible for the band observed experimentally at 1879.3 and 1896.8 cm^{-1} , respectively. The acetylene $\text{C}\equiv\text{C}$ stretch (ν_5 , 2029.5 cm^{-1}) is not observed in the spectrum of d_1 -phenylacetylene due to a drop in intensity upon deuteration, contrasting with the fairly strong feature observed in the standard isotopologue.

IV. CONCLUSIONS

Anharmonicity is intrinsically required for the accurate characterization of the vibrational spectrum of polycyclic aromatic hydrocarbons,¹⁶ a principle that is further supported by the results presented in the present study that covers frequencies from the mid- to far-infrared. For both phenylacetylene and d_1 -phenylacetylene, direct and indirect assignments are only possible by including anharmonic terms in the vibrational potential energy surface calculation. The mid- to far-IR spectra of these molecules are full of higher-order transitions such as overtones and combination bands, including both 2- and 3-quanta combination bands. So far, 3-quanta bands have not received much attention. The present study demonstrates, however, that inclusion of such transitions is necessary to come to a proper understanding of these spectra. Additionally, the use of polyad matrices to allow for intensity sharing is integral for the correct treatment of anharmonic intensities in PAHs. Combined with the

previous publication¹⁶ of the absorption spectra of phenylacetylene and d₁-phenylacetylene in the CH (CD) stretch fundamental region, the full absorption spectrum up to 3400 and 3100 cm⁻¹, respectively, excluding the 2300-2500 cm⁻¹ region that is outside of the laser frequency capabilities of FELIX, is now complete and included in Figure S3.

Overall, very good agreement is present between experiment and theory for both phenylacetylene and d₁-phenylacetylene with an average difference in frequency of 1.2 and 1.0%, respectively, for the directly assigned features. The low-frequency rocking and bending motions at approximately 500 cm⁻¹ and below have some of the largest differences in frequency with an average difference of 2.5 and 2.7%. These modes are notoriously difficult to characterize with computational methods, and all of them deviate in a similar manner. Even so, an assignment is still easy to make for all features due to the sparsity of features in this region. As described in Section III A, ν_{21} and $2\nu_{21}$ in phenylacetylene show the largest deviation in frequency between theory and experiment (3.8 and 6.1%) with the inaccuracy compounded for the overtone transition. This same deviation is not observed in d₁-phenylacetylene. The average difference on the order of 1% for these molecules is larger than that found for unsubstituted¹⁸ and methyl-substituted¹⁹ PAHs. This is not so surprising given the strong resonances present in phenylacetylene¹⁶ and the known difficulty in computing vibrational spectra of acetylene molecules.⁴³

Large isotopic frequency shifts are reported here for various modes that involve the acetylene hydrogen. Many of these modes either lose or gain intensity based on deuteration, causing major changes to the resultant absorption spectrum, particularly in the 500-900 cm⁻¹ (20-11.1 μm) range. Further experiments on isotopically labeled PAHs are needed, and such absorption experiments are currently underway in our laboratory. Even with the insights provided herein, there remain quite a number of unanswered questions regarding how deuteration impacts the emission of PAHs, especially with regards to the strong infrared bands observed in the 1-20 μm range.^{1,2,49} Very little PAH, and their deuterated isotopologues in particular, emission data exist in the literature. A recent emission experiment on phenylacetylene and d₁-phenylacetylene carried out by Lacinbala et al.,⁵⁰ and a follow-up computational study by our group¹⁶ look into the role that anharmonicity plays in the emission of substituted aromatic molecules. Outside of this recent example, there exists a dearth of experimental emission data for this wavelength region, requiring further experimental and computational investigation to understand how anharmonicity and the isotopic

frequency and intensity shifts impact the emission spectrum of standard and functionalized PAHs, molecules that are strongly tied to infrared observations pertinent to astronomical observation during the age of JWST and its possible successors.

V. SUPPLEMENTARY MATERIAL

The data that support the findings of this study are available in the supplemental information and from the corresponding author upon reasonable request.

ACKNOWLEDGMENTS

V.J.E. acknowledges an appointment to the NASA Postdoctoral Program at NASA Ames Research Center, administered by the Oak Ridge Associated Universities through a contract with NASA. C.B. is grateful for an appointment at NASA Ames Research Center through the San José State University Research Foundation (80NSSC22M0107). V.J.E, C.B., and R.F acknowledge support from the Internal Scientist Funding Model (ISFM) Laboratory Astrophysics Directed Work Package at NASA Ames. Computer time from the Pleiades cluster of the NASA Advanced Supercomputer (NAS) is gratefully acknowledged. R.C.F. acknowledges support from NASA grant NNH22ZHA004C and the Mississippi Center for Supercomputing Research supported in part from NSF Grant OIA-1757220. Studies of interstellar PAHs at Leiden Observatory are supported through a NWO Spinoza grant. The HFML-FELIX Laboratory is supported by the project CALIPSOplus under the Grant Agreement 730872 from the EU Framework Programme for Research and Innovation HORIZON 2020. We gratefully acknowledge the Nederlandse Organisatie voor Wetenschappelijk Onderzoek (NWO) and thank the FELIX staff.

REFERENCES

- ¹Alexander GGM Tielens. Interstellar polycyclic aromatic hydrocarbon molecules. *Annu. Rev. Astron. Astrophys.*, 46:289–337, 2008.
- ²C Boersma, L J Allamandola, V J Esposito, A Maragkoudakis, J D Bregman, P Temi, T J Lee, R C Fortenberry, and E Peeters. JWST: Deuterated PAHs, PAH Nitriles, and

- PAH Overtone and Combination Bands. I. Program Description and First Look. *The Astrophysical Journal*, 959(74), December 2023.
- ³Marie L Laury, Matthew J Carlson, and Angela K Wilson. Vibrational frequency scale factors for density functional theory and the polarization consistent basis sets. *Journal of computational chemistry*, 33(30):2380–2387, 2012.
- ⁴Stephen R. Langhoff. Theoretical Infrared Spectra for Polycyclic Aromatic Hydrocarbon Neutrals, Cations, and Anions. *The Journal of Physical Chemistry*, 100(8):2819–2841, January 1996.
- ⁵Charles W. Bauschlicher and Stephen R. Langhoff. The calculation of accurate harmonic frequencies of large molecules: the polycyclic aromatic hydrocarbons, a case study. *Spectrochimica Acta Part A: Molecular and Biomolecular Spectroscopy*, 53(8):1225–1240, July 1997.
- ⁶C. W. Bauschlicher, C. Boersma, A. Ricca, A. L. Mattioda, J. Cami, E. Peeters, F. Sánchez de Armas, G. Puerta Saborido, D. M. Hudgins, and L. J. Allamandola. THE NASA AMES POLYCYCLIC AROMATIC HYDROCARBON INFRARED SPECTROSCOPIC DATABASE: THE COMPUTED SPECTRA. *The Astrophysical Journal Supplement Series*, 189(2):341, August 2010. Publisher: The American Astronomical Society.
- ⁷Charles W. Bauschlicher, A. Ricca, C. Boersma, and L. J. Allamandola. The NASA Ames PAH IR Spectroscopic Database: Computational Version 3.00 with Updated Content and the Introduction of Multiple Scaling Factors. *The Astrophysical Journal Supplement Series*, 234(2):32, February 2018. Publisher: American Astronomical Society.
- ⁸O. Pirali, M. Vervloet, G. Mulas, G. Mallocci, and C. Joblin. High-resolution infrared absorption spectroscopy of thermally excited naphthalene. Measurements and calculations of anharmonic parameters and vibrational interactions. *Physical Chemistry Chemical Physics*, 11(18):3443–3454, April 2009. Publisher: The Royal Society of Chemistry.
- ⁹Fred M Behlen, Daniel B McDonald, V Sethuraman, and Stuart A Rice. Fluorescence spectroscopy of cold and warm naphthalene molecules: Some new vibrational assignments. *The Journal of Chemical Physics*, 75(12):5685–5693, 1981.
- ¹⁰E Cané, P PALMIER, R Tarroni, A Trombetti, and NC Handy. The high-resolution infrared spectra of naphthalene-h8 and naphthalene-d8: comparison of scaled scf and density functional force fields. *Gazzetta chimica italiana*, 126(5):289–296, 1996.

- ¹¹Joost M. Bakker, Britta Redlich, Alexander F. G. Van Der Meer, and Jos Oomens. INFRARED SPECTROSCOPY OF GAS-PHASE POLYCYCLIC AROMATIC HYDROCARBON CATIONS IN THE 10–50 μm SPECTRAL RANGE. *The Astrophysical Journal*, 741(2):74, November 2011.
- ¹²Jana Roithová, Juraj Jašík, Jesus J. Del Pozo Mellado, and Dieter Gerlich. Electronic spectra of ions of astrochemical interest: from fast overview spectra to high resolution. *Faraday Discussions*, 217(0):98–113, July 2019. Publisher: The Royal Society of Chemistry.
- ¹³Sandra D Wiersma, Alessandra Candian, Joost M Bakker, and Annemieke Petrignani. Gas-phase spectroscopy of photostable PAH ions from the mid- to far-infrared. *Monthly Notices of the Royal Astronomical Society*, 516(4):5216–5226, November 2022.
- ¹⁴Alexander K Lemmens, Piero Ferrari, Donatella Loru, Gayatri Batra, Amanda L Steber, Britta Redlich, Melanie Schnell, and Bruno Martinez-Haya. Wetting of a hydrophobic surface: Far-ir action spectroscopy and dynamics of microhydrated naphthalene. *J. Phys. Chem. Lett.*, --, 2023.
- ¹⁵Vincent J Esposito, Louis J Allamandola, Christiaan Boersma, Jesse D Bregman, Ryan C Fortenberry, Alexandros Maragkoudakis, and Pasquale Temi. Anharmonic IR absorption spectra of the prototypical interstellar PAHs phenanthrene, pyrene, and pentacene in their neutral and cation states. *Molecular Physics*, page e2252936, September 2023.
- ¹⁶Vincent J Esposito, Piero Ferrari, Wybren Jan Buma, Christiaan Boersma, Cameron J Mackie, Alessandra Candian, and Ryan C Fortenberry. Anharmonicity and deuteration in the IR absorption and emission spectrum of phenylacetylene. *Molecular Physics*, page e2261570, September 2023.
- ¹⁷Cameron J. Mackie, Alessandra Candian, Xinchuan Huang, Elena Maltseva, Annemieke Petrignani, Jos Oomens, Wybren Jan Buma, Timothy J. Lee, and Alexander G. G. M. Tielens. The anharmonic quartic force field infrared spectra of three polycyclic aromatic hydrocarbons: Naphthalene, anthracene, and tetracene. *The Journal of Chemical Physics*, 143(22):224314, December 2015.
- ¹⁸Cameron J. Mackie, Alessandra Candian, Xinchuan Huang, Elena Maltseva, Annemieke Petrignani, Jos Oomens, Andrew L. Mattioda, Wybren Jan Buma, Timothy J. Lee, and Alexander G. G. M. Tielens. The anharmonic quartic force field infrared spectra of five non-linear polycyclic aromatic hydrocarbons: Benz[a]anthracene, chrysene, phenanthrene,

- pyrene, and triphenylene. *The Journal of Chemical Physics*, 145(8):084313, August 2016.
- ¹⁹Cameron J. Mackie, Alessandra Candian, Xinchuan Huang, Elena Maltseva, Annemieke Petrigani, Jos Oomens, Wybren Jan Buma, Timothy J. Lee, and Alexander G. G. M. Tielens. The anharmonic quartic force field infrared spectra of hydrogenated and methylated PAHs. *Physical Chemistry Chemical Physics*, 20(2):1189–1197, January 2018. Publisher: The Royal Society of Chemistry.
- ²⁰Cameron J. Mackie, Tao Chen, Alessandra Candian, Timothy J. Lee, and Alexander G. G. M. Tielens. Fully anharmonic infrared cascade spectra of polycyclic aromatic hydrocarbons. *The Journal of Chemical Physics*, 149(13):134302, October 2018.
- ²¹Cameron J. Mackie, Alessandra Candian, Timothy J. Lee, and Alexander G. G. M. Tielens. Anharmonicity and the IR Emission Spectrum of Neutral Interstellar PAH Molecules. *The Journal of Physical Chemistry A*, 126(20):3198–3209, May 2022.
- ²²Shreyak Banhatti, Daniël B. Rap, Aude Simon, Heloïse Leboucher, Gabi Wenzel, Christine Joblin, Britta Redlich, Stephan Schlemmer, and Sandra Brünken. Formation of the acenaphthylene cation as a common C₂H₂-loss fragment in dissociative ionization of the PAH isomers anthracene and phenanthrene. *Physical Chemistry Chemical Physics*, 24(44):27343–27354, 2022.
- ²³Giacomo Mulas, Cyril Falvo, Patrick Cassam-Chenaï, and Christine Joblin. Anharmonic vibrational spectroscopy of polycyclic aromatic hydrocarbons (PAHs). *The Journal of Chemical Physics*, 149(14):144102, October 2018.
- ²⁴Ryan Chown, Ameet Sidhu, Els Peeters, Alexander GGM Tielens, Jan Cami, Olivier Berne, Emilie Habart, Felipe Alarcon, Amelie Canin, Ilane Schroetter, et al. Pdrs4all iv. an embarrassment of riches: Aromatic infrared bands in the orion bar. *arXiv preprint arXiv:2308.16733*, 2023.
- ²⁵Elena Maltseva, Annemieke Petrigani, Alessandra Candian, Cameron J. Mackie, Xinchuan Huang, Timothy J. Lee, Alexander G. G. M. Tielens, Jos Oomens, and Wybren Jan Buma. HIGH-RESOLUTION IR ABSORPTION SPECTROSCOPY OF POLYCYCLIC AROMATIC HYDROCARBONS: THE REALM OF ANHARMONICITY. *The Astrophysical Journal*, 814(1):23, November 2015. Publisher: The American Astronomical Society.
- ²⁶Elena Maltseva, Annemieke Petrigani, Alessandra Candian, Cameron J. Mackie, Xinchuan Huang, Timothy J. Lee, Alexander G. G. M. Tielens, Jos Oomens, and

- Wybren Jan Buma. HIGH-RESOLUTION IR ABSORPTION SPECTROSCOPY OF POLYCYCLIC AROMATIC HYDROCARBONS IN THE 3 μm REGION: ROLE OF PERIPHERY. *The Astrophysical Journal*, 831(1):58, October 2016. Publisher: The American Astronomical Society.
- ²⁷Elena Maltseva, Cameron J. Mackie, Alessandra Candian, Annemieke Petrignani, Xinchuan Huang, Timothy J. Lee, Alexander G. G. M. Tielens, Jos Oomens, and Wybren Jan Buma. High-resolution IR absorption spectroscopy of polycyclic aromatic hydrocarbons in the 3 μm region: role of hydrogenation and alkylation. *Astronomy & Astrophysics*, 610:A65, February 2018. Publisher: EDP Sciences.
- ²⁸AK Lemmens, DB Rap, JMM Thunnissen, CJ Mackie, A Candian, AGGM Tielens, AM Rijs, and WJ Buma. Anharmonicity in the mid-infrared spectra of polycyclic aromatic hydrocarbons: molecular beam spectroscopy and calculations. *Astronomy & Astrophysics*, 628:A130, 2019.
- ²⁹AK Lemmens, AM Rijs, and WJ Buma. Infrared spectroscopy of jet-cooled “grandpahs” in the 3–100 μm region. *The Astrophysical Journal*, 923(2):238, 2021.
- ³⁰Vincent J Esposito, Piero Ferrari, Wybren Jan Buma, Christiaan Boersma, Cameron J Mackie, Alessandra Candian, Ryan C Fortenberry, and Alexander GGM Tielens. Anharmonicity and deuteration in the ir absorption and emission spectrum of phenylacetylene. *Molecular Physics*, page e2261570, 2023.
- ³¹Donatella Loru, Carlos Cabezas, José Cernicharo, Melanie Schnell, and Amanda L Steber. Detection of ethynylbenzene in tmc-1 and the interstellar search for 1, 2-diethynylbenzene. *Astronomy & Astrophysics*, 677:A166, 2023.
- ³²Vasyl Yatsyna, Daniël J. Bakker, Peter Salén, Raimund Feifel, Anouk M. Rijs, and Vitali Zhaunerchyk. Infrared Action Spectroscopy of Low-Temperature Neutral Gas-Phase Molecules of Arbitrary Structure. *Physical Review Letters*, 117(11):118101, September 2016.
- ³³Sander Jaeqx, Jos Oomens, Alvaro Cimas, Marie-Pierre Gageot, and Anouk M. Rijs. Gas-Phase Peptide Structures Unraveled by Far-IR Spectroscopy: Combining IR-UV Ion-Dip Experiments with Born–Oppenheimer Molecular Dynamics Simulations. *Angewandte Chemie International Edition*, 53(14):3663–3666, 2014. eprint: <https://onlinelibrary.wiley.com/doi/pdf/10.1002/anie.201311189>.

- ³⁴Sjors Bakels, Marie-Pierre Gageot, and Anouk M Rijs. Gas-phase infrared spectroscopy of neutral peptides: Insights from the far-ir and thz domain. *Chemical reviews*, 120(7):3233–3260, 2020.
- ³⁵Axel D. Becke. Density-functional thermochemistry. III. The role of exact exchange. *The Journal of Chemical Physics*, 98(7):5648–5652, April 1993.
- ³⁶Vincenzo Barone, Paola Cimino, and Emiliano Stendardo. Development and Validation of the B3LYP/N07D Computational Model for Structural Parameter and Magnetic Tensors of Large Free Radicals. *Journal of Chemical Theory and Computation*, 4(5):751–764, May 2008.
- ³⁷M. J. Frisch, G. W. Trucks, H. B. Schlegel, G. E. Scuseria, M. A. Robb, J. R. Cheeseman, G. Scalmani, V. Barone, G. A. Petersson, H. Nakatsuji, et al. Gaussian 16, 2016.
- ³⁸Vincenzo Barone, Malgorzata Biczysko, and Julien Bloino. Fully anharmonic IR and Raman spectra of medium-size molecular systems: accuracy and interpretation. *Physical Chemistry Chemical Physics*, 16(5):1759–1787, January 2014. Publisher: The Royal Society of Chemistry.
- ³⁹Vincenzo Barone. Anharmonic vibrational properties by a fully automated second-order perturbative approach. *The Journal of Chemical Physics*, 122(1):014108, January 2005.
- ⁴⁰Ryan C. Fortenberry and Timothy J. Lee. Chapter Six - Computational vibrational spectroscopy for the detection of molecules in space. In David A. Dixon, editor, *Annual Reports in Computational Chemistry*, volume 15, pages 173–202. Elsevier, January 2019.
- ⁴¹Peter R. Franke, John F. Stanton, and Gary E. Douberly. How to VPT2: Accurate and Intuitive Simulations of CH Stretching Infrared Spectra Using VPT2+K with Large Effective Hamiltonian Resonance Treatments. *The Journal of Physical Chemistry A*, 125(6):1301–1324, February 2021. Publisher: American Chemical Society.
- ⁴²J. K. G. Watson. *On Vibrational Spectra and Structure*. Elsevier, Amsterdam, 1977.
- ⁴³Ryan C. Fortenberry and Timothy J. Lee. Vibrational and Rovibrational Spectroscopy Applied to Astrochemistry. In *Vibrational Dynamics of Molecules*, pages 235–295. WORLD SCIENTIFIC, July 2022.
- ⁴⁴J. F. Gaw, A. Willets, W. H. Green, and N. C. Handy. SPECTRO: A Program for the Derivation of Spectroscopic Constants From Provided Quartic Force Fields and Cubic Dipole Fields. In Joel M. Bowman and Mark A. Ratner, editors, *Advances in Molecular Vibrations and Collision Dynamics*, pages 170–185. JAI Press, Inc., Greenwich, Connecticut,

- 1991.
- ⁴⁵Jan M. L. Martin and Peter R. Taylor. Accurate ab initio quartic force field for trans-HNNH and treatment of resonance polyads. *Spectrochimica Acta Part A: Molecular and Biomolecular Spectroscopy*, 53(8):1039–1050, July 1997.
- ⁴⁶Jan M. L. Martin, Timothy J. Lee, Peter R. Taylor, and Jean-Pierre François. The Anharmonic Force Field of Ethylene, C₂H₄, by Means of Accurate ab Initio Calculations. *J. Chem. Phys.*, 103(7):2589–2602, 1995.
- ⁴⁷Timothy J. Lee and Ryan C. Fortenberry. The unsolved issue with out-of-plane bending frequencies for CC multiply bonded systems. *Spectrochimica Acta Part A: Molecular and Biomolecular Spectroscopy*, 248:119148, March 2021.
- ⁴⁸Ryan C. Fortenberry, Timothy J. Lee, and Holger S. P. Müller. Excited vibrational level rotational constants for SiC₂: A sensitive molecular diagnostic for astrophysical conditions. *Molecular Astrophysics*, 1:13–19, November 2015.
- ⁴⁹E. Peeters, S. Hony, C. Van Kerckhoven, A. G. G. M. Tielens, L. J. Allamandola, D. M. Hudgins, and C. W. Bauschlicher. The rich 6 to 9 m spectrum of interstellar PAHs. *Astronomy & Astrophysics*, 390(3):1089–1113, August 2002. Number: 3 Publisher: EDP Sciences.
- ⁵⁰Ozan Lacinbala, Géraldine Féraud, Julien Vincent, and Thomas Pino. Aromatic and Acetylenic C–H or C–D Stretching Bands Anharmonicity Detection of Phenylacetylene by UV Laser-Induced Vibrational Emission. *The Journal of Physical Chemistry A*, 126(30):4891–4901, August 2022.